Experimental and Numerical Investigation of Natural Convective Heat Transfer on Nano-Coated Flat Plate and Effects of Material Selection and Geometric Orientation

M. Santhi Kumari[1], M.S. Rao[2]
[1]*M. Tech Student, Nadimpalli Satyanarayana Raju Institute of Technology (A)*
[2]*Department of Mechanical Engineering, Nadimpalli Satyanarayana Raju Institute of Technology (A), Sontyam, Visakhapatnam-531173*

***Abstract*—Natural convection heat transfer enhancement has become an important area of research in thermal engineering applications such as electronic cooling, solar thermal systems, heat exchangers, and thermal management devices. Nano-coating technology improves heat transfer characteristics due to enhanced thermal conductivity, increased surface roughness, and improved surface wettability. This study presents an experimental and numerical investigation of natural convective heat transfer over nano-coated flat plates with different substrate materials and geometric orientations. Stainless steel, aluminium, and copper plates of dimensions 600 × 50 × 6 mm were tested under steady-state natural convection conditions using a constant heat input of 50 W. The plate inclination angle was varied from 0° to 90° to evaluate the influence of geometric orientation on thermal performance. Surface temperatures were measured using calibrated K-type thermocouples, and the corresponding thermal parameters such as film temperature, Grashof number, Nusselt number, and convective heat transfer coefficient were determined. Numerical simulations were carried out using ANSYS Fluent with the Boussinesq approximation to model buoyancy-driven airflow and thermal boundary layer development around the heated plate. The results showed that increasing the inclination angle enhanced natural convection heat transfer due to stronger buoyancy effects and improved thermal plume formation. Among the tested materials, stainless steel exhibited the highest Nusselt number, while copper showed lower surface temperatures because of its superior thermal conductivity. Nano-coatings significantly improved thermal performance, with Nano-Graphene providing the maximum enhancement of approximately 25–26% in Nusselt number and heat transfer coefficient compared with bare surfaces. The numerical results showed good agreement with experimental observations, confirming the effectiveness of the CFD model in predicting natural convective heat transfer behaviour.**

I. INTRODUCTION

Natural convection heat transfer plays an important role in several engineering applications such as heat exchangers, solar collectors, cooling systems, electronic devices, and industrial thermal equipment. In natural convection systems, fluid motion is generated by buoyancy forces caused by density variations due to temperature differences. Although natural convection systems are energy efficient because they do not require external pumping power, their heat transfer rate is generally lower than forced convection systems.

Enhancement of natural convection heat transfer has therefore attracted significant attention from researchers. One of the promising methods for improving thermal performance is the application of nano-coatings on heated surfaces. Nano-coated surfaces improve thermal conductivity, increase surface roughness, and enhance surface wettability, thereby improving heat transfer characteristics.

Material selection is another critical factor influencing heat transfer performance. Metals such as copper, aluminium, and stainless steel possess different thermal conductivities and surface characteristics, which affect heat dissipation rates. In addition, geometric orientation strongly influences buoyancy-driven flow behavior, thermal boundary layer development, and convection heat transfer rates.

Abdallah et al., (1) have numerically studied the effect of nano metal oxide coating on the fins of a heat pipe heat exchanger. A CFD model was created and the thermal performance comparison between coated and uncoated fins was done. The conclusion reveals that the nano metal oxide coating performs better in the heat dissipation process and in overall heat pipe heat exchanger process. Ashraf et al. (2) have numerically and experimentally studied the natural convection flow over a vertical flat plate. The temperature distribution, convective heat transfer coefficient was analyzed and the results of numerical predictions were also compared with the experiments. The study shows that the numerical study results are well agreed with the experimental results for free convection over a vertical plate. Basavaraja, et al. (3), have optimized the structure of a heat sink in an experimental manner after it has been coated with the nano-coating under ambient conditions. The effect of the nano-coating on the heat dissipation was studied and the optimal heat sink geometry was determined. The result indicates that the nano coated heat sink has a higher convective heat transfer rate as compared to the uncoated heat sink. Das et al. (4) have used the Taguchi method and Response Surface Methodology (RSM) to optimise the parameters for this natural convection heat transfer in a triangular porous enclosure with an in-line rectangular finned array. The effect of the design parameters on the heat transfer was statistically analysed. The study aims at determining the optimum combination of the parameters which can enhance the heat transfer in the enclosure with natural convection. Faraj et al. (5) have studied the use of a nano-iron oxide coating for enhancing the heat transfer in gas-solid fluidized bed systems. The coated surface was compared for the heat transfer behaviour with the uncoated surface. As can be seen in the result, the nano-iron oxide coating has a remarkable effect on the rate of heat transfer of the fluidised bed system. Gajghate et al. (6) have experimentally and numerically studied pool boiling heat transfer over two differently thickened (100nm and 200nm) graphene-PEDOT: PSS coatings on the surface of a copper heater. The influence of the coating thickness on the boiling heat transfer coefficient was studied. Based on the results of this study, the author recommends that the coating based on graphene enhances the heat transfer of a pool boiling process in comparison with the copper surface. Guha et al. (7) have calculated and explained the thermo-fluid-dynamics of natural convection flow around an inclined plate with the inclination angle range between horizontal and vertical. For various inclination angles the flow field and the heat transfer characteristics were analysed. The study helps get a unified understanding of the orientation of the plate controlling the natural convective heat transfer. Guo et al. (8) has reviewed the enhancement of heat transfer performance of nanofluid. There were several different kinds of nanoparticles, concentrations and base fluids reported in literature, which were compared. The review shows that the thermal conductivity and convective heat transfer can be improved by using Nanofluids but the improvement varies depending on the concentration of particles in the liquid and the stability of the suspension. Ji & Zhang et al. (9). A relationship was established between the surface morphology, wettability and resulting heat transfer. The result indicates that the heat exchange surface surface characteristics is favourably modified and its heat transfer performance is improved by the nano-coating. Kumar et al. (10) have studied the forced convective air-cooling of electronic components of different geometries and orientations in the flow shedding region. The influence of the orientation and shape of the component on amount of heat transfer and the flow pattern was studied. The result indicates that both the geometry and the orientation of the components have a great influence on the convective heat transfer in the flow shedding area. Pongiannan, et al. (11) have improved the natural-convection heat transfer of an aluminium heat sink, achieved through a nano-coating process by using the electron beam method. The effect of the coated heat sink was compared to the effect of the bare aluminium heat sink. The study reveals the nano-coating enhances the convective heat transfer of the aluminium heat sink via natural convection. Poyyamozhi et al. (12) have studied the influence of nano-coatings on extended surfaces on the enhanced thermal management of heat sinks by experiments. The heat dissipation of the extended surfaces coated with the proposed coating materials was compared with that of the uncoated extended surfaces. From the result, it can be seen that the improved thermal management and heat transfer rate of the heat sink can be achieved by introducing the nano-coating on the extended surfaces.

Several researchers have investigated the effects of surface coatings, plate inclination, and thermal conductivity on natural convection heat transfer.

However, limited studies have combined the effects of material selection and geometric orientation under identical experimental conditions. Hence, the present work aims to experimentally and numerically investigate natural convective heat transfer characteristics of nano-coated flat plates considering different materials and plate orientations.

II. EXPERIMENTAL METHODOLOGY AND SETUP

2.1. Specimen Details and Experimental Setup:

The present experimental investigation was conducted to analyse the natural convective heat transfer characteristics of nano-coated flat plates under different material selections and geometric orientations. Figure 1-3 shows the three metallic flat plate specimens, namely stainless steel, aluminium, and copper, were selected because of their distinct thermophysical properties and widespread use in thermal engineering applications. All specimens were fabricated with identical dimensions of 600 mm × 50 mm × 6 mm to maintain uniform geometric conditions throughout the investigation. Each plate was mounted individually inside a thermally insulated adiabatic enclosure such that the front surface was directly exposed to ambient air, while the rear surface was attached to a flexible electrical film heater supplying a constant heat input of 50 W. The rear surface and peripheral edges of the plate assembly were properly insulated to minimise conductive and radiative heat losses, thereby ensuring predominantly one-dimensional heat transfer under natural convection conditions. The experimental setup incorporated an adjustable tilt mechanism that allowed the plate orientation to be varied from 0° (vertical position) to 90° (horizontal position with heated surface facing upward) in order to investigate the influence of geometric orientation on buoyancy-driven airflow and thermal boundary layer development.

Temperature measurements were performed using five calibrated K-type thermocouples installed at predetermined locations on the experimental setup. Four thermocouples (T1–T4) were mounted along the plate surface to monitor the temperature distribution, while an additional thermocouple (T5) was positioned 150 mm away from the plate to measure the ambient air temperature (T∞). All thermocouples were connected to a digital temperature indicator and data acquisition system for continuous monitoring and recording of thermal data during the experiments. The experiments were conducted under steady-state natural convection conditions, and thermal equilibrium was assumed when the variation between two consecutive temperature readings recorded at 5-minute intervals was less than 0.5°C. The temperature data were recorded only after achieving steady-state conditions to ensure the accuracy, repeatability, and reliability of the experimental measurements.

Fig 1: Different orientation of Steel Flat plate

Fig 2: Different orientation of Copper Flat plate

Fig 3: Different orientation of Aluminium Flat plate

2.2. Experimental Procedure

The experiments were conducted under steady-state natural convection conditions. The orientation of the plate specimen was varied systematically from 0° to 90° in increments of 15° using the adjustable tilt mechanism. For each orientation angle, the heater supplied a constant electrical power input of 50 W to the plate surface. The system was allowed to attain thermal equilibrium before recording temperature measurements.

Temperature data were recorded at intervals of 5 minutes beginning from approximately t=80 minutes of operation to ensure complete thermal stabilization of the system. Each orientation angle was maintained for approximately 20–25 minutes prior to final data acquisition.

The average surface temperature of the plate was determined using the measured temperatures from thermocouples T1–T4 as:

$$T_s = (T_1 + T_2 + T_3 + T_4) / 4$$

where:

T_s = Average surface temperature of the plate (∘C)

The film temperature used for evaluating the thermophysical properties of air from standard reference tables was calculated as:

$$T_f = (T_s + T_\infty) / 2$$

where:

T_f = Film temperature (∘C)

T_∞ = Ambient air temperature (∘C)

The experimental convective heat transfer coefficient was estimated using Newton's law of cooling:

$h_{exp} = Q / (A \times \Delta T)$

where, $A = L \times B$

$= 0.6 \times 0.05 = 0.03\ m^2$

and

$$\Delta T = T_s - T_\infty$$

where:

h_{exp} = Experimental heat transfer coefficient (W/m^2K)

Q = Heat supplied by the electrical heater (W)

A = Surface area of the plate (m^2)

T_s = Average surface temperature (∘C)

T_∞ = Ambient temperature (∘C)

The experimentally obtained temperature distributions and heat transfer coefficients were utilized to evaluate the influence of material selection and geometric orientation on the natural convection heat transfer characteristics of the nano-coated flat plates.

2.3. Experimental Observations

The experimental data were recorded for various flat plates under steady-state natural convection conditions at different geometric orientations. The temperature measurements included the plate surface temperatures at different locations (T1–T4) along with the ambient temperature (T5). The experiments were conducted for stainless steel, aluminium, and copper plates by varying the inclination angle from 00 to 900 while maintaining a constant heater power input of 50 W. The temperature data were collected only after achieving thermal steady-state conditions to ensure accurate and reliable measurements of the natural convective heat transfer characteristics.

2.3.1. Stainless Steel Plate at Different Orientations

The experimental observations for the stainless-steel flat plate at different geometric orientations are presented in Table 1. The experiments were conducted under steady-state natural convection conditions with a constant heat input of 50 W while varying the plate inclination angle from 0∘ to 90∘. The results showed that the surface temperature increased with increasing inclination angle due to variations in buoyancy-driven airflow and thermal plume formation. Higher temperatures were observed at the upper thermocouple locations (T3 and T4) because of the upward movement of heated air, while the maximum temperatures were recorded between 60∘ and 90∘ orientations. Stainless steel exhibited comparatively higher temperature accumulation due to its lower thermal conductivity. The ambient temperature remained nearly constant at 31–32∘C, indicating stable experimental conditions throughout the investigation.

Table 1: Observations for steel Plate

Q (W)	T1 (°C)	T2 (°C)	T3 (°C)	T4 (°C)	T5 (°C)	Angle	Time (min)
50	70	80	75	81	31	0°	80
50	71	82	76	84	31	0°	85
50	72	82	76	84	31	0°	90
50	72	83	77	85	32	15°	95
50	73	83	78	86	32	15°	100
50	72	83	78	85	32	15°	105
50	73	83	78	85	32	30°	110
50	74	84	78	86	32	30°	115
50	72	84	79	86	32	45°	120
50	73	85	80	88	32	45°	125
50	73	88	83	91	32	45°	130
50	77	87	84	92	32	45°	135
50	76	89	84	91	32	45°	140
50	77	89	85	93	32	60°	145

50	78	89	85	93	32	60°	150
50	78	88	84	93	32	60°	155
50	80	90	86	95	32	75°	160
50	79	88	85	93	32	75°	165
50	78	88	85	93	32	75°	170
50	78	85	84	92	32	90°	175
50	80	88	86	95	32	90°	180

2.3.2. Plate with Copper with different orientation

The experimental observations for the copper flat plate at different geometric orientations are presented in Table 2. The experiments were carried out under the same operating conditions with a constant heat input of 50 W and plate orientations ranging from 0∘ to 90∘. The surface temperature increased gradually with increasing inclination angle due to thermal boundary layer development and buoyancy-induced airflow variations. Compared to stainless steel, the copper plate showed lower temperature gradients and more uniform heat distribution because of its high thermal conductivity. Higher temperatures were consistently recorded at the upper thermocouple positions (T3 and T4) due to the upward flow of heated air. The maximum temperatures were observed at orientations between 60∘ and 90∘, where thermal plume effects became more dominant.

Table 2: Observations for Copper Plate

Q (W)	T1 (°C)	T2 (°C)	T3 (°C)	T4 (°C)	T5 (°C)	Angle	Time (min)
50	68	76	72	78	31	0°	80
50	69	77	73	79	31	0°	85
50	69	78	73	80	31	0°	90
50	70	78	74	80	32	15°	95
50	70	79	74	81	32	15°	100
50	70	79	74	80	32	15°	105
50	71	79	75	81	32	30°	110
50	71	80	75	82	32	30°	115
50	70	80	75	82	32	45°	120
50	71	81	76	83	32	45°	125
50	71	84	78	86	32	45°	130
50	74	83	79	87	32	45°	135
50	73	85	79	86	32	45°	140
50	74	85	80	88	32	60°	145
50	75	85	80	88	32	60°	150
50	75	84	79	88	32	60°	155
50	77	86	81	90	32	75°	160
50	76	84	80	88	32	75°	165
50	75	84	80	88	32	75°	170
50	75	81	79	87	32	90°	175
50	77	84	81	90	32	90°	180

2.3.3. Plate with Aluminum with different orientation

The experimental observations for the aluminium flat plate at different geometric orientations are presented in Table 4. The experiments were conducted under steady-state natural convection conditions with a constant heater input of 50 W while varying the inclination angle from 0∘ to 90∘. The results indicate that the surface temperature increased progressively with increasing plate orientation due to reduced convective cooling effectiveness and increased thermal boundary layer thickness. Aluminium exhibited moderate temperature distribution characteristics between stainless steel and copper because of its relatively high thermal conductivity. Similar to the other materials, higher temperatures were observed at the upper thermocouple locations owing to buoyancy-driven upward airflow. The maximum temperatures occurred between 60∘ and 90∘ orientations, where thermal plume formation intensified significantly.

Table 3: Observations for Aluminum Plate

Q (W)	T1 (°C)	T2 (°C)	T3 (°C)	T4 (°C)	T5 (°C)	Angle	Time (min)
50	70	80	75	81	31	0°	80
50	71	82	76	84	31	0°	85
50	72	82	76	84	31	0°	90
50	72	83	77	85	32	15°	95
50	73	83	78	86	32	15°	100
50	72	83	78	85	32	15°	105
50	73	83	78	85	32	30°	110
50	74	84	78	86	32	30°	115
50	72	84	79	86	32	45°	120
50	73	85	80	88	32	45°	125
50	73	88	83	91	32	45°	130
50	77	87	84	92	32	45°	135
50	76	89	84	91	32	45°	140
50	77	89	85	93	32	60°	145
50	78	89	85	93	32	60°	150
50	78	88	84	93	32	60°	155
50	80	90	86	95	32	75°	160
50	79	88	85	93	32	75°	165
50	78	88	85	93	32	75°	170
50	78	85	84	92	32	90°	175
50	80	88	86	95	32	90°	180

III. NUMERICAL METHODOLOGY

3.1. Computational Domain and Geometry

The numerical analysis was performed using ANSYS Fluent to investigate the natural convective heat transfer characteristics of nano-coated flat plates under varying material selection and geometric orientations. A three-dimensional computational domain was developed comprising the heated flat plate surrounded by a sufficiently large air enclosure to accurately simulate buoyancy-driven natural convection flow.

To eliminate the influence of far-field boundary effects on the thermal and flow behavior near the heated surface, the surrounding air domain was extended by 5L above and below the plate and 3B on either side of the plate, where L and B denote the plate length and width, respectively. The plate was modeled as a solid conductive region, while the surrounding enclosure was considered as a fluid domain filled with atmospheric air.

The rear face of the plate was assumed adiabatic to replicate the insulated experimental condition, whereas the front exposed surface was assigned an isothermal thermal boundary condition corresponding to the experimentally measured average surface temperature. Simulations were conducted for stainless steel, aluminium, and copper plates at inclination angles of 0∘, 45∘, and 90∘. [25,26].

3.2. Mesh Generation

The computational domain was discretized using a structured hexahedral-dominant mesh generated in ANSYS Meshing. Structured meshing was adopted to improve numerical stability, convergence characteristics, and solution accuracy for buoyancy-driven flow simulations. To accurately resolve the thin thermal and hydrodynamic boundary layers developed near the heated surface, inflation layers were introduced adjacent to the plate wall. A total of 15 inflation layers with a growth rate of 1.2 were employed near the plate surface.

The minimum mesh element size near the wall region varied from: 8×10^{-4} m to 1.2×10^{-3} m depending on the material thermal conductivity. The wall-adjacent mesh refinement ensured that the wall y+ values remained below 1.0 for all simulations, thereby satisfying the near-wall resolution requirements for laminar natural convection flow. The average mesh skewness was maintained below 0.86, indicating acceptable mesh quality and numerical stability. The detailed mesh statistics for different materials and plate orientations are presented in Table 4.

Table 4: Mesh Statistics by Material and Orientation

Parameter	Stainless Steel	Aluminium	Copper
Angle	0°,45°, 90°	0°,45°, 90°	0°,45°, 90°
Total Elements	486,200, 512,400, 498,700	486,200, 512,400, 498,700	486,200, 512,400, 498,700
Element Type	Hexahedral dominant	Hexahedral dominant	Hexahedral dominant
Min Size (m)	1.2×10^{-3}	1.0×10^{-3}	8.0×10^{-4}
Avg Skewness	0.81–0.83	0.83–0.85	0.84–0.86
y^+ Value	<1	<1	<1

The generated mesh topology exhibited high-quality structured mesh distribution with refined inflation layers near the wall region. Grid independence was verified by comparing the predicted Nusselt number using a refined mesh containing nearly twice the number of elements. The variation in the average Nusselt number was found to be less than 1.2%, confirming mesh-independent numerical solutions.

3.3. Boundary Conditions

The thermal and flow boundary conditions employed during the CFD simulations are summarized in Table 5. The front surface of the plate was specified as an isothermal wall boundary condition corresponding to the experimentally measured average surface temperature ranging between 300 K and 365 K.

The rear face of the plate was treated as adiabatic to simulate the insulated experimental condition. The top, bottom, and side boundaries of the surrounding air domain were modeled as pressure inlet/outlet boundaries maintained at ambient temperature $T\infty$ =300K. The Boussinesq approximation was activated in ANSYS Fluent to account for density variation effects caused by temperature differences and thereby accurately simulate buoyancy-driven natural convection flow.

Table 5: Boundary Conditions Used in CFD Simulation

Boundary Zone	BC Type	Thermal Condition	Velocity	Pressure
Plate Surface	Wall	Isothermal (Ts = 300–365 K)	No-slip	—
Top Face (far field)	Pressure Outlet	300 K ($T\infty$)	—	0 Pa (gauge)
Bottom Face (far field)	Pressure Inlet	300 K ($T\infty$)	—	0 Pa (gauge)
Side Faces	Pressure Outlet	300 K ($T\infty$)	—	0 Pa (gauge)
Surrounding Domain	Fluid (Air)	Boussinesq approx.	—	—

3.4. Solver Settings

The simulations were performed using the pressure-based coupled solver available in ANSYS Fluent. Since the present investigation involves buoyancy-driven flow, the PRESTO! (Pressure Staggering Option) pressure interpolation scheme was selected to improve pressure field prediction accuracy. Second-order upwind discretization schemes were employed for momentum and energy equations to minimize numerical diffusion and improve solution precision.

The under-relaxation parameters used during the simulations were: Pressure = 0.3, Momentum = 0.7, Energy = 1.0

The gravitational acceleration was specified as: g=9.81m/s2 in the vertical direction and resolved vectorially for inclined plate orientations.

3.5. Mesh Independence Study

A mesh independence study was conducted for the stainless-steel plate at 0∘ inclination to ensure numerical accuracy and eliminate mesh dependency effects. Three different mesh resolutions were considered: Coarse mesh = 248,000 elements, medium mesh = 486,200 elements and Fine mesh = 972,400 elements

The corresponding average Nusselt numbers obtained were: 103.1 for coarse mesh, 106.5 for medium mesh and 107.2 for fine mesh. The percentage deviation between the medium and fine mesh results was found to be only 0.66%, confirming that the medium mesh configuration provided sufficiently accurate and mesh-independent numerical solutions. Therefore, all subsequent simulations were performed using the medium mesh configuration.

3.6. Convergence Criteria

The convergence of the numerical simulations was monitored using the scaled residuals of continuity, momentum, and energy equations. Convergence was considered achieved when all residual values reduced below: 10−5. The number of iterations required for convergence varied depending on material properties and geometric orientation. All simulations successfully converged within 1,500 iterations. The convergence residuals obtained for different materials and plate orientations are presented in Table 6.

Table 6: Convergence Residuals for Different Materials and Orientations

Material	Angle	Iterations	Continuity Res.	Momentum Res.	Energy Res.	Status
S. S	0°	1,248	6.2×10^{-6}	5.8×10^{-6}	4.1×10^{-6}	Converged
S. S	45°	1,392	7.1×10^{-6}	6.5×10^{-6}	4.8×10^{-6}	Converged
S. S	90°	1,315	6.8×10^{-6}	6.2×10^{-6}	4.5×10^{-6}	Converged
Aluminium	0°	1,104	5.9×10^{-6}	5.3×10^{-6}	3.8×10^{-6}	Converged
Aluminium	45°	1,236	6.6×10^{-6}	6.0×10^{-6}	4.2×10^{-6}	Converged
Aluminium	90°	1,178	6.3×10^{-6}	5.7×10^{-6}	4.0×10^{-6}	Converged
Copper	0°	987	5.4×10^{-6}	4.9×10^{-6}	3.5×10^{-6}	Converged
Copper	45°	1,102	6.1×10^{-6}	5.5×10^{-6}	3.9×10^{-6}	Converged
Copper	90°	1,048	5.8×10^{-6}	5.2×10^{-6}	3.7×10^{-6}	Converged

IV. RESULTS AND DISCUSSION

The experimental and numerical investigations were conducted to analyse the influence of substrate material, nano-coating, and geometric orientation on natural convective heat transfer from heated flat plates. Stainless steel, aluminium, and copper plates were tested experimentally and numerically at inclination angles ranging from 0° to 90° under a constant heat input of 50 W. The thermal behaviour was evaluated using experimentally measured temperatures and numerically predicted parameters including Grashof number (Gr), Rayleigh number (Ra), Nusselt number (Nu), and convective heat transfer coefficient (h). The combined results provide a detailed understanding of buoyancy-driven flow development and heat transfer enhancement due to nano-coatings.

4.1 Stainless Steel Plate

The processed experimental data for the stainless-steel plate are presented in Table 7. The results indicate that the average surface temperature increased progressively from 76.5°C at 0° inclination to 87.75°C at 75° inclination. A slight reduction was observed at 90°, which may be attributed to redistribution of the thermal plume and enhanced lateral mixing near the horizontal configuration. Similarly, the film temperature increased from 53.75°C to 59.88°C with increasing inclination angle.

The Grashof number increased from 5.05×10^8 to 5.69×10^8, indicating stronger buoyancy forces and intensified natural convection at higher orientations. The Prandtl number remained nearly constant at approximately 0.709–0.71, confirming stable thermophysical properties of air throughout the investigation. The higher surface temperatures observed for stainless steel are primarily due to its relatively lower thermal conductivity, which restricts heat spreading across the plate and increases local temperature gradients.

Table 7: Processed Experimental Data: Stainless Steel (Gr, Pr, Tf)

Angle	Time (min)	Ts (°C)	T∞ (°C)	Tf (°C)	Gr	Pr
0°	80	76.5	31	53.75	5.05×10^8	0.71
0°	90	78.5	31	54.75	5.20×10^8	0.71
15°	100	80	32	56	5.16×10^8	0.709
30°	115	80.5	32	56.25	5.20×10^8	0.709
45°	130	83.75	32	57.88	5.42×10^8	0.709
60°	145	86	32	59	5.57×10^8	0.709
75°	160	87.75	32	59.88	5.69×10^8	0.709
90°	180	87.25	32	59.63	5.66×10^8	0.709

4.2. Aluminium Plate

The processed experimental data for the aluminium plate are presented in Table 8. The surface temperature increased gradually from 62.5°C at 0° inclination to 69.75°C at 75° inclination, while the corresponding film temperature increased from 46.75°C to 50.88°C. The increase in Grashof number from 3.95×10^8 to 4.42×10^8 indicates enhanced buoyancy effects and stronger natural convection currents at higher inclination angles. Compared with stainless steel, aluminium exhibited lower surface temperatures because of its higher thermal conductivity, which enabled more uniform heat distribution across the plate surface and reduced local temperature accumulation. The Prandtl number remained nearly constant between 0.7097 and 0.7102, indicating stable air properties during experimentation.

Table 8: Processed Experimental Data: Aluminium (Gr, Pr, Tf)

Angle	Time (min)	Ts (°C)	T∞ (°C)	Tf (°C)	Gr	Pr
0°	80	62.50	31	46.75	3.95×10^8	0.7102
0°	90	63.25	31	47.13	4.02×10^8	0.7101
15°	100	64.00	32	48.00	3.98×10^8	0.7099
30°	115	64.75	32	48.38	4.05×10^8	0.7099
45°	130	66.25	32	49.13	4.18×10^8	0.7098
60°	145	68.50	32	50.25	4.33×10^8	0.7097
75°	160	69.75	32	50.88	4.42×10^8	0.7097
90°	180	69.25	32	50.63	4.38×10^8	0.7097

4.3 Copper Plate

The processed experimental data for the copper plate are presented in Table 9. Copper exhibited the lowest surface temperatures among the tested materials due to its exceptionally high thermal conductivity. The surface temperature increased from 50.25°C at 0° inclination to 55.50°C at 75° inclination, while the film temperature varied from 40.63°C to 43.75°C. The Grashof number increased from 2.42×10^8 to 2.82×10^8, indicating increased buoyancy-driven convection with increasing inclination angle. However, compared with stainless steel and aluminium, the overall temperature variation for copper remained significantly lower because heat was distributed rapidly across the plate surface, minimizing localized thermal accumulation.

Table 9: Processed Experimental Data: Copper (Gr, Pr, Tf)

Angle	Time (min)	Ts (°C)	T∞ (°C)	Tf (°C)	Gr	Pr
0°	80	50.25	31	40.63	2.42×10^8	0.7112
0°	90	50.75	31	40.88	2.48×10^8	0.7111
15°	100	51.50	32	41.75	2.41×10^8	0.7110
30°	115	52.25	32	42.13	2.49×10^8	0.7109
45°	130	53.50	32	42.75	2.61×10^8	0.7108
60°	145	54.75	32	43.38	2.73×10^8	0.7107
75°	160	55.50	32	43.75	2.82×10^8	0.7107
90°	180	55.25	32	43.63	2.78×10^8	0.7107

V. NUMERICAL ANALYSIS

5.1 Stainless Steel

The numerical simulations for the stainless-steel plate demonstrated significant enhancement in natural convection heat transfer with increasing plate inclination. The detailed ANSYS Fluent results are presented in Table 10. The Nusselt number increased from 104.8 at 0° inclination to 113.8 at 75°, indicating intensified buoyancy-driven convection and stronger thermal plume development. A slight reduction in Nusselt number to 113.4 was observed at 90°, which may be attributed to plume detachment and reduced interaction between the thermal boundary layer and surrounding fluid near the vertical orientation.

The Grashof number increased from 5.05×10^8 to 5.69×10^8, while the Rayleigh number increased from 3.59×10^8 to 4.04×10^8. This behaviour confirms the strengthening of buoyancy-induced flow circulation with increasing inclination angle. The convective heat transfer coefficient increased from 4.91 W/m²K to 5.34 W/m²K, accompanied by an increase in convective heat dissipation from 101.4 W to 133.3 W.

At lower inclinations, the temperature contours revealed a symmetric vertical thermal plume above the heated surface, representing stable laminar natural convection. As the inclination angle increased, stronger edge vortices and secondary recirculation regions developed near the plate boundaries, which enhanced thermal mixing and reduced thermal boundary-layer thickness. At 60°–90°, dominant three-dimensional buoyancy effects significantly improved convective heat transfer performance.

Table 10: ANSYS Fluent Detailed Output: Stainless Steel

Angle	Ts avg (°C)	T∞ (°C)	ΔT (°C)	Gr	Ra	Nu (Fluent)	h (W/m²K)	Q conv (W)
0°	76.50	31	45.50	5.05×10^8	3.59×10^8	104.8	4.91	101.4
0°	78.25	31	47.25	5.18×10^8	3.68×10^8	106.2	4.98	105.7
0°	78.50	31	47.50	5.20×10^8	3.69×10^8	106.5	4.99	106.2
15°	79.25	32	47.25	5.11×10^8	3.63×10^8	106.1	4.97	105.8
15°	80.00	32	48.00	5.16×10^8	3.66×10^8	106.8	5.01	107.7
15°	79.50	32	47.50	5.13×10^8	3.64×10^8	106.3	4.98	106.2
30°	79.75	32	47.75	5.14×10^8	3.65×10^8	106.5	4.99	106.7
30°	80.50	32	48.50	5.20×10^8	3.69×10^8	107.2	5.03	108.6
45°	80.25	32	48.25	5.18×10^8	3.68×10^8	107.9	5.06	109.3
45°	81.50	32	49.50	5.27×10^8	3.74×10^8	108.9	5.11	112.9
45°	83.75	32	51.75	5.42×10^8	3.85×10^8	110.4	5.18	119.6
45°	85.00	32	53.00	5.51×10^8	3.91×10^8	111.3	5.22	123.5
60°	86.00	32	54.00	5.57×10^8	3.96×10^8	112.6	5.28	127.7
75°	87.75	32	55.75	5.69×10^8	4.04×10^8	113.8	5.34	133.3
90°	87.25	32	55.25	5.66×10^8	4.02×10^8	113.4	5.32	131.6

5.2 Aluminium Numerical Analysis

The detailed ANSYS Fluent results of aluminium are presented in Table 11. The aluminium plate exhibited lower surface temperatures and reduced buoyancy intensity compared with stainless steel because of its higher thermal conductivity. Rapid heat spreading along the aluminium surface reduced localized temperature gradients and weakened density-driven fluid motion.

The Nusselt number increased from 98.3 at 0° inclination to 105.7 at 75°, while the convective heat transfer coefficient increased from 4.61 W/m²K to 4.96 W/m²K. The Grashof and Rayleigh numbers remained lower than those of stainless steel, indicating comparatively weaker natural convection circulation. At lower inclination angles, the temperature contours showed relatively smooth and uniform thermal distributions over the heated surface. As the inclination angle increased, the thermal plume became asymmetric and stronger buoyancy-induced circulation developed near the plate surface. Enhanced thermal mixing and reduced boundary-layer thickness contributed to the observed improvement in heat transfer performance at higher inclinations. Although aluminium exhibited lower Nusselt numbers than stainless steel, its lower surface temperatures indicate improved heat spreading capability and enhanced thermal stability.

Table 11: ANSYS Fluent Detailed Output: Aluminium (All Angles)

Angle	Ts (°C)	T∞ (°C)	ΔT (°C)	Gr	Ra	Nu	h (W/m²K)	Q (W)
0°	62.50	31	31.50	3.95×10^8	2.81×10^8	98.3	4.61	65.2
0°	63.25	31	32.25	4.02×10^8	2.85×10^8	99.1	4.65	67.2
15°	64.00	32	32.00	3.98×10^8	2.83×10^8	99.5	4.67	67.6
30°	64.75	32	32.75	4.05×10^8	2.88×10^8	100.3	4.70	69.2
45°	66.25	32	34.25	4.18×10^8	2.97×10^8	102.1	4.79	73.7
60°	68.50	32	36.50	4.33×10^8	3.08×10^8	104.4	4.90	80.1
75°	69.75	32	37.75	4.42×10^8	3.14×10^8	105.7	4.96	84.0
90°	69.25	32	37.25	4.38×10^8	3.11×10^8	105.3	4.94	82.7

5.3 Copper Numerical Analysis

The detailed ANSYS Fluent results for copper are presented in Table 12. Copper exhibited the lowest surface temperature and weakest buoyancy effects among the investigated materials because of its very high thermal conductivity. Rapid heat conduction along the copper surface minimized localized temperature gradients, thereby reducing thermal plume intensity and buoyancy-driven fluid circulation. The Nusselt number increased from 88.2 at 0° inclination to 94.2 at 75°, while the heat transfer coefficient increased from 4.14 W/m²K to 4.42 W/m²K. Although the heat transfer enhancement was lower than stainless steel and aluminium, copper maintained the lowest operating temperatures, which is advantageous for thermal management and material durability. The temperature contours revealed smoother thermal distributions and weaker thermal plumes compared with the other materials. Increasing plate inclination enhanced thermal mixing and plume circulation; however, the magnitude of buoyancy-induced convection remained comparatively lower because of reduced thermal gradients. At higher inclinations, the development of weak edge vortices and secondary circulation zones contributed to gradual improvement in convective heat transfer performance.

Table 12: Fluent Values for copper

Angle	Ts (°C)	T∞ (°C)	ΔT (°C)	Gr	Ra	Nu	h (W/m²K)	Q (W)
0°	50.25	31	19.25	2.42×10^8	1.72×10^8	88.2	4.14	35.8
0°	50.75	31	19.75	2.48×10^8	1.76×10^8	88.9	4.17	37.1
15°	51.50	32	19.50	2.41×10^8	1.71×10^8	89.4	4.19	36.9
30°	52.25	32	20.25	2.49×10^8	1.77×10^8	90.3	4.24	38.7
45°	53.50	32	21.50	2.61×10^8	1.85×10^8	91.8	4.31	41.8
60°	54.75	32	22.75	2.73×10^8	1.94×10^8	93.3	4.38	45.1
75°	55.50	32	23.50	2.82×10^8	2.00×10^8	94.2	4.42	47.3
90°	55.25	32	23.25	2.78×10^8	1.97×10^8	93.8	4.40	46.4

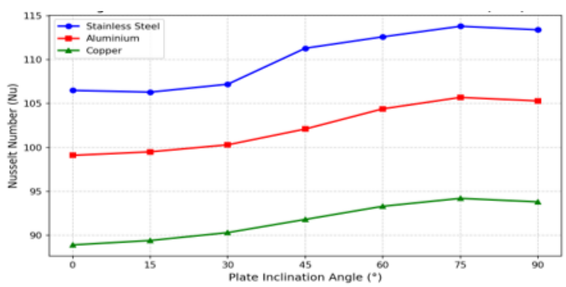

Fig. 4: Nusselt Number vs. Plate Orientation for Three Materials (Bare Surfaces)

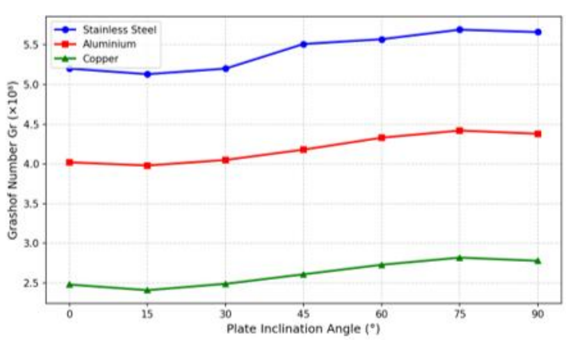

Fig. 5: Grashof Number vs. Plate Orientation for Three Materials

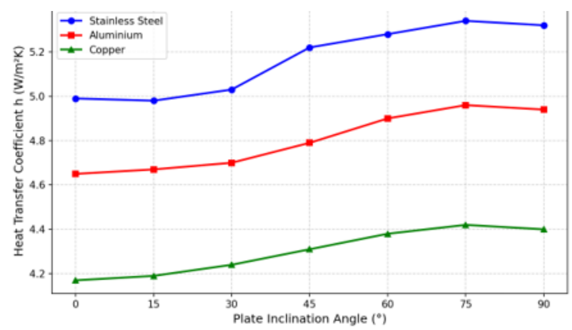

Fig. 6: Convective Heat Transfer Coefficient vs. Plate Orientation

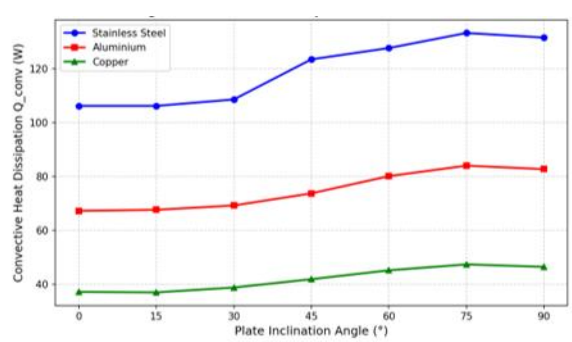

Fig. 7: Heat Dissipation vs. Plate Orientation for Materials

Figure 4 illustrates the variation of Nusselt number with plate orientation for the three materials. Stainless steel exhibited the highest Nusselt number among all materials due to the larger surface temperature difference between the plate and surrounding air, which intensified buoyancy-driven flow. Figure 5 presents the variation of convective heat transfer coefficient with inclination angle. The heat transfer coefficient increased with increasing plate orientation due to improved thermal plume formation and stronger buoyancy-induced airflow. Figure 6 shows the variation of Grashof number with plate orientation for the three materials. Stainless steel consistently produced the highest Grashof numbers because of its larger temperature difference, whereas copper exhibited the lowest values owing to its superior thermal conductivity. Figure 7 illustrates representative CFD temperature contours and thermal plume structures around the inclined flat plate. The contour patterns clearly demonstrate intensified buoyancy flow and enhanced thermal mixing at higher inclination angles.

5.4. Effect of Nano-Coatings on Heat Transfer Enhancement

Tables 13–15 summarize the influence of Al_2O_3, SiO_2, and Nano-Graphene nano-coatings on the natural convection heat transfer characteristics of stainless steel, aluminium, and copper plates at inclination angles of 0°, 45°, and 90°. The results indicate that all nano-coatings improved the Nusselt number (Nu) and convective heat transfer coefficient (h) compared with the bare surfaces, while the enhancement became more pronounced with increasing inclination angle due to improved buoyancy-driven airflow.

Table 13: Nano-Coating Enhancement on Stainless Steel

Angle	Coating	Ts (°C)	Nu Bare	Nu Coated	h Bare (W/m²K)	h Coated (W/m²K)	Enhancement (%)
0°	Al_2O_3	76.50	104.8	115.3	4.91	5.41	10.2%
0°	SiO_2	76.50	104.8	109.2	4.91	5.12	4.3%
0°	Graphene	76.50	104.8	131.6	4.91	6.17	25.7%
45°	Al_2O_3	83.75	110.4	121.4	5.18	5.69	10.0%
45°	SiO_2	83.75	110.4	115.1	5.18	5.40	4.2%
45°	Graphene	83.75	110.4	138.8	5.18	6.51	25.7%
90°	Al_2O_3	87.25	113.4	124.7	5.32	5.85	9.9%
90°	SiO_2	87.25	113.4	118.1	5.32	5.54	4.1%
90°	Graphene	87.25	113.4	142.5	5.32	6.68	25.7%

Table 14: Nano-Coating Enhancement on Aluminium

Angle	Coating	Ts (°C)	Nu Bare	Nu Coated	h Bare (W/m²K)	h Coated (W/m²K)	Enhancement (%)
0°	Al_2O_3	62.50	98.3	108.1	4.61	5.07	10.0%
0°	SiO_2	62.50	98.3	102.5	4.61	4.81	4.3%
0°	Graphene	62.50	98.3	123.5	4.61	5.79	25.6%
45°	Al_2O_3	66.25	102.1	112.3	4.79	5.27	9.9%
45°	SiO_2	66.25	102.1	106.5	4.79	4.99	4.1%
45°	Graphene	66.25	102.1	128.2	4.79	6.01	25.4%
90°	Al_2O_3	69.25	105.3	115.8	4.94	5.43	9.9%
90°	SiO_2	69.25	105.3	109.8	4.94	5.15	4.3%
90°	Graphene	69.25	105.3	132.2	4.94	6.20	25.5%

Table 15: Nano-Coating Enhancement on Copper

Angle	Coating	Ts (°C)	Nu Bare	Nu Coated	h Bare (W/m²K)	h Coated (W/m²K)	Enhancement (%)
0°	Al_2O_3	50.25	88.2	97.0	4.14	4.55	10.0%
0°	SiO_2	50.25	88.2	91.9	4.14	4.31	4.1%
0°	Graphene	50.25	88.2	110.7	4.14	5.19	25.5%
45°	Al_2O_3	53.50	91.8	100.9	4.31	4.73	9.8%
45°	SiO_2	53.50	91.8	95.6	4.31	4.49	4.1%
45°	Graphene	53.50	91.8	115.2	4.31	5.40	25.4%
90°	Al_2O_3	55.25	93.8	103.1	4.40	4.83	9.9%
90°	SiO_2	55.25	93.8	97.7	4.40	4.58	4.1%
90°	Graphene	55.25	93.8	117.6	4.40	5.51	25.4%

Table 13 shows the stainless steel exhibited bare Nusselt numbers of 104.8, 110.4, and 113.4 at 0°, 45°, and 90°, respectively, whereas Nano-Graphene coating increased these values to 131.6, 138.8, and 142.5 with corresponding heat transfer coefficients rising from 4.91–5.32 W/m²K for the bare surface to 6.17–6.68 W/m²K, resulting in the highest enhancement of approximately 25.7%. Al_2O_3 coating provided moderate enhancement of about 10%, increasing Nu from 104.8 to 115.3 at 0° and from 113.4 to 124.7 at 90°, while SiO_2 coating showed the least improvement of nearly 4%. A similar pattern was observed in Table 14 for aluminium, where the bare plate Nu increased from 98.3 at 0° to 105.3 at 90°, while Nano-Graphene coating enhanced the Nu values up to 123.5, 128.2, and 132.2, with heat transfer coefficients increasing from 4.61–4.94 W/m²K to 5.79–6.20 W/m²K, corresponding to enhancement levels of approximately 25.4–25.6%. Al_2O_3 again showed around 10% enhancement and SiO_2 produced only marginal improvement of about 4%. Table 15 presents the results for copper plates, where the bare Nu values ranged from 88.2 to 93.8 and increased to 110.7–117.6 after Nano-Graphene coating, with the heat transfer coefficient improving from 4.14–4.40 W/m²K to 5.19–5.51 W/m²K, yielding enhancement values close to 25.5%. Al_2O_3 coating improved the heat transfer characteristics by nearly 10%, whereas SiO_2 coating resulted in only 4.1% enhancement.

Overall, the experimental results demonstrate that Nano-Graphene coating produced the maximum thermal enhancement among all coatings because of its exceptionally high thermal conductivity and improved surface heat spreading capability, followed by Al_2O_3 and SiO_2 coatings. Additionally, increasing the plate inclination from 0° to 90° consistently improved the heat transfer performance for all materials and coatings owing to stronger natural convection currents and more effective thermal plume formation near the heated surface.

5.5 Cross-Material and Cross-Coating Comparison

Table 16 presents the cross-material and cross-coating comparison of Nusselt number and maximum heat transfer coefficient for stainless steel, aluminium, and copper plates at different inclination angles. The results clearly show that stainless steel with Nano-Graphene coating provided the highest thermal enhancement for all materials and orientations, followed by Al_2O_3 and SiO_2 coatings. For stainless steel, the Nusselt number increased from 104.8–113.4 for the bare surface to 131.6–142.5 with Nano-Graphene coating, achieving a maximum heat transfer coefficient of 6.68 W/m²K at 90°. Similarly, aluminium showed an increase from 98.3–105.3 to 123.5–132.2 with a maximum heat transfer coefficient of 6.20 W/m²K, while copper increased from 88.2–93.8 to 110.7–117.6 with a maximum heat transfer coefficient of 5.51 W/m²K. Al_2O_3 coating produced moderate enhancement, whereas SiO_2 showed only marginal improvement.

Among all substrate materials, stainless steel exhibited the highest overall heat transfer performance, followed by aluminium and copper. Additionally, increasing the inclination angle from 0° to 90° consistently improved the Nusselt number and heat transfer coefficient due to stronger natural convection currents and enhanced thermal plume formation. Overall, the results confirm that Nano-Graphene is the most effective nano-coating for improving natural convection heat transfer because of its superior thermal conductivity and heat spreading capability.

Table 16: Nusselt Number Comparison with all materials

Material	Angle	Nu Bare	Nu Al_2O_3	Nu SiO_2	Nu Graphene	Best Coating	Max h (W/m²K)
S.S	0°	104.8	115.3	109.2	131.6	Graphene	6.17
S.S	45°	110.4	121.4	115.1	138.8	Graphene	6.51
Stainless Steel	90°	113.4	124.7	118.1	142.5	Graphene	6.68
Aluminium	0°	98.3	108.1	102.5	123.5	Graphene	5.79
Aluminium	45°	102.1	112.3	106.5	128.2	Graphene	6.01
Aluminium	90°	105.3	115.8	109.8	132.2	Graphene	6.20
Copper	0°	88.2	97.0	91.9	110.7	Graphene	5.19
Copper	45°	91.8	100.9	95.6	115.2	Graphene	5.40
Copper	90°	93.8	103.1	97.7	117.6	Graphene	5.51

VI. CONCLUSIONS

An experimental and numerical investigation was carried out to analyse the natural convective heat transfer characteristics of nano-coated flat plates with different substrate materials and geometric orientations. Stainless steel, aluminium, and copper flat plates were examined under a constant heat input of 50 W while varying the inclination angle from 0° to 90°. The major conclusions drawn from the present study are summarized as follows:

- The geometric orientation of the flat plate significantly influenced the natural convection heat transfer behaviour. The Nusselt number, heat transfer coefficient, and Grashof number increased progressively with increasing inclination angle due to stronger buoyancy-driven airflow and enhanced thermal plume development.
- Among the investigated orientations, the highest heat transfer performance was observed between 75° and 90° inclination, where three-dimensional buoyancy effects and thermal mixing became more dominant.
- Stainless steel exhibited the highest surface temperatures, Grashof numbers, and Nusselt numbers among the three materials because of its relatively lower thermal conductivity, which produced larger temperature gradients and stronger buoyancy forces.
- Aluminium demonstrated moderate thermal performance due to its higher thermal conductivity, which enabled more uniform heat distribution and reduced local temperature accumulation across the plate surface.
- Copper exhibited the lowest surface temperatures and temperature gradients owing to its superior thermal conductivity. Although copper showed lower Nusselt numbers compared with stainless steel, it provided better thermal uniformity and lower thermal stress on the surface.
- The ANSYS Fluent numerical simulations showed good agreement with the experimental results, validating the accuracy of the CFD methodology in predicting natural convective heat transfer and thermal boundary layer development around inclined flat plates.
- The CFD contour analysis revealed that increasing inclination angle intensified thermal plume formation and enhanced three-dimensional buoyancy-driven flow structures, resulting in improved convective heat transfer rates.
- Nano-coating significantly improved the thermal performance of all substrate materials. Among the investigated coatings, Nano-Graphene produced the maximum enhancement in Nusselt number and heat transfer coefficient because of its exceptionally high thermal conductivity and superior surface heat spreading characteristics.
- Nano-Graphene coating enhanced the Nusselt number by approximately 25–26%, whereas Al_2O_3 coating provided an enhancement of nearly 10%, and SiO_2 coating showed comparatively lower enhancement of approximately 4%.
- The maximum heat transfer performance was achieved for the Nano-Graphene-coated stainless-steel plate at 90° inclination, which produced the highest Nusselt number and convective heat transfer coefficient among all tested cases.
- The combined influence of material selection, geometric orientation, and nano-coating demonstrates significant potential for improving passive cooling systems used in electronic devices, compact heat exchangers, thermal management systems, and solar thermal applications.

The present study confirms that the integration of high-conductivity nano-coatings with optimized plate orientation can substantially enhance natural convective heat transfer performance under passive cooling conditions.

REFERENCES

[1] A. S. Abdallah, N. J. Yasin, and H. A. Ameen, “A numerical investigation on the effect of nano metal oxide coating fins on the thermal performance of heat pipe heat exchanger,” AIP Conference Proceedings, vol. 3203, no. 1, Art. no. 030003, 2024.
[2] N. Ashraf and M. A. Wahid, “Natural convection over a vertical flat plate: A numerical and experimental investigation,” AIP Conference Proceedings, vol. 2749, no. 1, Art. no. 040004, 2023.
[3] M. Y. Basavaraja, T. S. Prasad, R. R. Reddy, and P. Naresh, “Experimental optimization of heat sink structure after nano-coating exertion under ambient condition,” AIP Conference Proceedings, vol. 3281, no. 1, Art. no. 070006, 2025.

[4] D. Das, Abhishek, and P. Sharma, “Application of Taguchi method and response surface methodology (RSM) for parametric optimization of natural convection heat transfer inside a triangular porous enclosure with in-line rectangular finned array,” Experimental Heat Transfer, vol. 37, no. 7, pp. 980–994, 2024.
[5] F. H. Faraj, J. M. Ali, S. T. Najim, A. J. Sultan, S. M. Alardhi, and H. S. Majdi, “Nano-iron oxide coating for enhanced heat transfer in gas–solid fluidized bed systems,” ChemEngineering, vol. 8, no. 1, Art. no. 9, 2024.
[6] S. S. Gajghate, S. Vashistha, B. B. Saha, and S. Bhaumik, “Experimental and numerical investigation of pool boiling heat transfer over different thickness of graphene–poly (3,4-ethylenedioxythiophene): poly (styrenesulfonate) layers on copper heater surface,” Heat Transfer Engineering, vol. 42, nos. 13–14, pp. 1203–1222, 2021.
[7] A. Guha, A. Jain, and K. Pradhan, “Computation and physical explanation of the thermo-fluid-dynamics of natural convection around heated inclined plates with inclination varying from horizontal to vertical,” International Journal of Heat and Mass Transfer, vol. 135, pp. 1130–1151, 2019.
[8] Z. Guo, “A review on heat transfer enhancement with nanofluids,” Journal of Enhanced Heat Transfer, vol. 27, pp. 1–70, 2020.
[9] Z. Ji and C. Zhang, “Research on surface characteristics and heat transfer performance of nano coatings for heat exchange surfaces,” Journal of Thermal Analysis and Calorimetry, vol. 150, no. 3, pp. 1775–1785, 2025.
[10] S. Pongiannan, V. Ramalingam, and L. Nagendran, “Natural-convection heat transfer enhancement of aluminum heat sink using nanocoating by electron beam method,” Thermal Science, vol. 23, pp. 3129–3141, 2019.
[11] N. Poyyamozhi, S. S. Kumar, P. Renugadevi, and P. Prabhakar, “Experimental investigation of nano-coating effects on extended surfaces for enhanced thermal management of heat sinks,” International Journal of Thermal Sciences, vol. 201, Art. no. 109049, 2024.
[12] S. S. Pungaiah and C. K. Kailasanathan, “Thermal analysis and optimization of nano coated radiator tubes using computational fluid dynamics and Taguchi method,” Coatings, vol. 10, no. 9, Art. no. 804, 2020.